Macular Ganglion Cell Layer Imaging in Preperimetric Glaucoma with Speckle-Noise-Reduced Spectral-Domain Optical Coherence Tomography

(133/135)

Noriko Nakano, MD, Masanori Hangai, MD, Hideo Nakanishi, MD, Satoshi Mori, MD, Masayuki Nukada, MD, Yuriko Kotera, MD, Hanako Ikeda, MD, Hajime Nakamura, MD, Atsushi Nonaka, MD, Nagahisa Yoshimura, MD

Department of Ophthalmology and Visual Sciences, Kyoto University Graduate School of Medicine, 54 Kawahara-cho, Shogoin, Sakyo-ku, Kyoto 606-8507, Japan

This study was presented at the American Academy of Ophthalmology Annual Meeting, October 2009; San Francisco, California, U.S.A. and received the Best Poster Award.

Proprietary interest statement:
Masanori Hangai is a paid advisory board member for NIDEK CO., LTD., and received consulting fees from Topcon Corporation, and Nagahisa Yoshimura is a paid advisory board member for NIDEK CO., LTD., and is a paid advisory board member for Topcon Corporation.
None of the other authors has a conflict of interest to disclose.

Running head: Macular GCL Imaging in Preperimetric Glaucoma

Support: This research was partially supported by a Grant-in-Aid for Scientific Research (20592038) from the Japan Society for the Promotion of Science (JSPS).

Correspondence to
Masanori Hangai, MD, Department of Ophthalmology and Visual Sciences, Kyoto University Graduate School of Medicine, 54 Kawahara-cho, Shogoin, Sakyo-ku, Kyoto 606-8507, Japan

E-mail: hangai@kuhp.kyoto-u.ac.jp

Abstract (349/350)

Objective: To visualize the macular ganglion cell layer (GCL) and measure its thickness in normal eyes and eyes with preperimetric glaucoma, using speckle-noise-reduced spectral-domain optical coherence tomography (SD-OCT).

Design: Retrospective consecutive case series.

Participants: Thirty-seven eyes of 37 patients with preperimetric glaucoma and 39 normal eyes of 39 volunteers.

Methods: Vertical and horizontal SD-OCT B-scan images were acquired with minimal speckle noise by using eye-tracking to obtain and average 50 B-scans at each identical location of interest. B-scan images were manually analyzed for GCL, retinal nerve fiber layer (RNFL), and inner plexiform layer (IPL) shapes and thicknesses in the macula.

Main Outcome Measures: Macular GCL images and thickness in normal eyes and in eyes with preperimetric glaucoma.

Results: The macular GCL was clearly seen on speckle-noise-reduced SD-OCT images in normal eyes and eyes with preperimetric glaucoma. In each eye with preperimetric glaucoma, thinning of the macular GCL was visually apparent particularly on vertical scans. The mean regional macular GCL was most severely thinned in the inferior perifoveal region, where its thickness was less than 70% of its normal thickness in 30 (81.1%) of the 37 eyes and less than 50% of its normal thickness in 13 (35.1%) of the 37 eyes. When the sensitivity and specificity for detecting abnormal thinning (outside the lower limit of 99% confidence interval [CI] for the means in the 39 normal eyes) in at least one 0.5-mm segment or sector were compared, the macular GCL on vertical B-scans exhibited higher sensitivity (81.1%) than the other layers on vertical

B-scans (5.4–59.5%, *P* = 0.00075–0.021), the macular GCL (40.5%, *P* = 0.00027) on horizontal B-scans, the other layers (5.4%–48.6%, *P* < 0.00048–0.004) on horizontal B-scans, and circumpapillaty RNFL automatically measured on SD-OCT (54.1%, *P* = 0.021), and scanning laser polarimetry with variable corneal compensation (24.3%; *P* = 0.00095). All the macular layers on both the vertical and horizontal B-scans and cpRNFL thickness exhibited comparable specificity (91.4–100.0%, statistically not different).

Conclusions: Speckle-noise-reduced SD-OCT imaging allowed clear visualization and measurement of the macular GCL, which was severely thinned in eyes with preperimetric glaucoma.

In glaucoma, retinal ganglion cell (RGC) loss occurs as a result of damage to the RGC axons within the optic nerve head, and this loss then leads to visual field defects. The results of histological studies of enucleated eyes of patients with glaucoma by Quigley, et al.[1] and Kerrigan-Baumrind, et al.[2] and eyes of primates with experimental glaucoma by Harwerth, et al.[3] indicate that considerable loss of RGCs has occurred by the time alterations in visual function (visual field deficits) are detected clinically. This is consistent with clinical findings that glaucomatous structural changes detectable in the optic nerve head and retinal nerve fiber layer (RNFL) can precede detectable visual field deficits.[3-9] Thus, direct assessment of the RGCs in patients might be ideal for understanding the damage in eyes with "preperimetric" (before visual field changes) glaucoma. However, studies of RGC loss due to glaucoma in human eyes have been limited to histological approaches using enucleated eyes, because no noninvasive methods are currently available to view individual living RGCs.

Loss of RGCs likely leads to atrophy of the ganglion cell layer (GCL). About 50% of the RGC somas are concentrated in the macula; subsequently, the macular GCL comprises multilayered RGC somas that generate a thick configuration. Furthermore, the axons of not only macular RGCs but also those of some peripheral RGCs outside the macula pass through the macular area to reach the optic nerve head. Thus, the macular GCL and RNFL may be promising targets with different characteristics for noninvasive imaging to clinically assess RGC loss. Many previous studies showed that the macula becomes atrophic in eyes with glaucoma when measured using optical imaging modalities.[10-19] Furthermore, recent studies showed that it is the innermost 3 to 4 layers in the macula that are atrophic in glaucoma, especially in preperimetric glaucoma, when measured using optical coherence tomography (OCT).[20-24] These results strongly suggest that the macular GCL and RNFL have become atrophic by the time alterations in visual function become

evident clinically. However, although it is possible to visualize and measure macular RNFL on OCT images,[25] it has been difficult to actually visualize the shape and thickness of the GCL on OCT images because of inability to identify the boundary between the GCL and inner plexiform layer (IPL) with confidence.

Two factors could account for this boundary being obscured on OCT images obtained to date: the image resolution limits of the OCT equipment used and speckle noise.[26] Because the mean thickness of macular GCL is greater than 30 μm,[21] much greater than the axial resolution limit of standard OCT, axial resolution of the equipment used would not fully account for the poor visibility of the GCL boundary in OCT B-scan images. In fact, although ultrahigh-resolution (UHR; ~3 μm) imaging using a laboratory OCT system improved visualization of the GCL in the macula compared to the standard resolution of time-domain (TD)-OCT systems, the boundary between the GCL and IPL was still unclear, even using UHR-OCT. [27,28] Thus, speckle noise, which is the primary artifact in OCT images and arises from the interference of coherent waves backscattered from nearby scatterers, could be the major factor,[29-32] and indeed, our and others' studies showed that effective reduction of speckle noise using spectral-domain OCT (SD-OCT) dramatically improves visualization of the boundaries of the GCL.[26,31]

With SD-OCT, B-scan images can be acquired 45 to 130 times faster than with TD-OCT, and when the SD-OCT system includes a 3-dimensional eye-tracking system (Spectralis™ HRA+OCT, Heidelberg Engineering, Heidelberg, Germany), it is possible to obtain up to 50 to 100 B-scans at the exact same location. Averaging these numerous B-scans obtained at the same location results in sufficient reduction in speckle noise to show the GCL boundary clearly.

The purpose of this pilot study was to determine whether the morphology of the macular GCL in normal eyes and eyes with preperimetric glaucoma could be visualized and its thickness measured on

speckle-noise-reduced vertical and horizontal B-scans obtained using the Spectralis SD-OCT in normal eyes and eyes with preperimetric glaucoma.

METHODS

All investigations in this study adhered to the tenets of the Declaration of Helsinki and the study was approved by the Institutional Review Board and Ethics Committee of Kyoto University Graduate School of Medicine. Informed consent for examinations was obtained from all participants.

Candidates for this study were patients with preperimetric glaucoma who underwent Spectralis SD-OCT at Kyoto University Hospital (Kyoto, Japan) between July 14, 2008, and June 15, 2009, and volunteers with healthy eyes. Preperimetric glaucoma was defined as evident glaucomatous appearance of the optic nerve head in eyes with normal visual fields. Volunteer eyes were categorized as normal if they had an intraocular pressure (IOP) of 21 mmHg or less, a normal-appearing optic disc head, and normal results with visual field testing.

Exclusion criteria for both groups were best-corrected visual acuity (BCVA) worse than 20/20 in the Snellen equivalent, equivalent refractive error of more than 3 diopters (D) or < −6 D, unreliable visual field results (fixation loss > 20%, false-positive > 15% or false-negative > 33%) on standard automated perimetry (SAP) using the Humphrey 24-2 Swedish Interactive Threshold Algorithm (SITA) (HFA, Carl Zeiss Meditec, Dublin, CA), evidence of vitreoretinal disease, or diabetes mellitus or any other systemic disease that might affect the eye.

Ocular examinations performed on patients at the first visit included automated refractive keratometry, measurements of uncorrected visual acuity (VA) and BCVA using the 5-meter Landolt chart,

slit-lamp examinations, IOP measurements using a Goldmann applanation tonometer, standard automated perimetry (SAP), Heidelberg Retina Tomography II (HRT II, Heidelberg Engineering), scanning laser polarimetry with variable corneal compensation (GDx-VCC, Carl Zeiss Meditec), dilated funduscopy, stereo disc photography using a 3-Dx simultaneous stereo disc camera (Nidek, Gamagori, Japan), and Spectralis SD-OCT.

Visual Field Testing

Reliable visual field test results (fixation loss ≤ 20%; false positives ≤ 15% and false negatives ≤ 33%) on standard automated perimetry (SAP), using the Humphrey 24-2 Swedish Interactive Threshold Algorithm (SITA) (HFA, Carl Zeiss Meditec) were used. Visual field defects caused by glaucoma were defined, on the basis of SAP results, as (1) abnormal range on the glaucoma hemifield test or (2) a pattern standard deviation (PSD) of <5% from the normal reference. Results were confirmed by 2 consecutive tests.

Optic Disc Evaluation

The appearance of the optic nerve head on fundus photographs, including the stereoscopic photographs, was independently evaluated by 3 glaucoma specialists (MH, HOI, and AN) who were masked to all other data about the eyes. Images of each eye were displayed on a monitor for each eye from both normal and preperimetric glaucoma candidates. Glaucomatous optic nerve head appearance was defined as the presence of diffuse or localized rim thinning, disc hemorrhage, or a vertical cup-to-disc ratio of 0.2 or greater than that in the fellow eye. If the decisions of all 3 examiners were not in agreement, consensus was reached by group review and discussion of the fundus color photographs and stereophotographs.

Speckle-Noise-Reduced SD-OCT

Horizontal and vertical speckle-noise-reduced SD-OCT imaging centered on the fovea centralis was performed using the Spectralis™ HRA+OCT.[26] Each A-scan of this instrument had a depth of 2 mm and comprised 512 pixels, providing a digital depth sampling of 3.9 μm per pixel. Each B-scan for this study spanned 30° (approximately 9 mm) and consisted of 1,536 A-scans (acquired at a rate of 40,000 per second), providing a digital transverse sampling resolution of 5 μm per pixel. The combination of high-resolution scanning laser imaging of the retina and SD-OCT enables real-time 3-dimensional tracking of eye movements and real-time averaging of multiple B-scans acquired at each identical location of interest on the retina to reduce speckle noise. Radial scans centered at the fovea or vertical serial scans were also obtained.

Hand Delineation of Retinal Layer Boundaries and Thickness Measurements

The boundaries of the RNFL (vitreoretinal interface and the border between RNFL and GCL), GCL (the borders between RNFL and GCL and between GCL and IPL), and inner plexiform layer (IPL) (the borders between GCL and IPL and between IPL and the inner nuclear layer) were drawn on SD-OCT B-scan images by 2 independent delineators at the Kyoto OCT Reading Center[33] who were masked to all clinical information using custom-made functions written into the standard built-in Spectralis™ HRA+OCT software by Heidelberg engineers. The delineators marked areas of “fringe washout” where shadows from blood vessels prevented visualization of underlying structures and where retinal layers were disrupted or deformed by blood vessels or their shadows. Where the structure of intraretinal layers was disrupted in this way, the

delineators connected by a straight line the end points of each boundary line on either side of the disruption.

Inter-Delineator Variability Assessment

To assess inter-delineator variability, raw results obtained independently by 2 delineators were compared. To assess the accuracy of the delineations of each delineator for each eye, a third independent observer (NN), who was also masked to clinical information about the eyes, joined the group review with the 2 delineators to check the boundary lines. If both the 2 delineators' results were judged to be accurate by group review, one of the results was randomly selected for use in analysis. If one of the 2 delineators' results was judged to be inaccurate by group review, the other boundary line was selected for use in analysis. If both the 2 delineators' results were judged inaccurate, the review group decided how they should be corrected; once corrected, 1 result was arbitrarily chosen for inclusion. To visualize inter-delineator variability, we superimposed the mean raw GCL thickness data of the 2 delineators in a graph. To display the symmetry along the horizontal and vertical B-scans, we also superimposed the mean arbitrated GCL thickness data in the nasal–temporal and superior–inferior hemispheres.

After manual delineation of retinal layer boundaries, Spectralis software was used to measure thicknesses of each layer by calculating the distance in pixels between that layer's inner and outer boundary lines and converting the result to micrometers. The custom software displays a single thickness value on each A-scan (e.g., every 0.5-mm point from the foveal center) and a mean thickness value that is averaged within each defined region (macula, superior, and inferior hemisphere, parafovea [0.5–1.5 mm from the foveal center] and perifovea [1.5–3.0 mm from the foveal center], and every 0.5-mm segment).

To determine if thickness measurements in eyes with preperimetric glaucoma differed from those

for normal eyes in individual eyes, after checking normal distribution of thickness values in normal eyes, we computed 95% and 99% confidence intervals (CIs) for the mean thickness of each layer in the normal study eyes. Thickness measurements in the eyes with preperimetric glaucoma were then categorized on the basis of thickness measurements obtained for the normal eyes: "normal," measurement within the 95% CI values for the mean thickness in normal eyes; “borderline thickened,” between the upper 95% and upper 99% CI limit for the mean in normal eyes; “borderline thin,” between the lower 95% and lower 99% CI limit for the mean in normal eyes; “abnormally thick,” above the upper 99% CI limit for the mean in normal eyes; or “abnormally thin,” below the lower 99% CI limit for the mean in normal eyes.

Automated Circumpapillary RNFL Thickness Measurements

GDx-VCC and Spectralis were used to assess circumpapillary RNFL (cpRNFL) thickness. For both instruments, cpRNFL thickness was automatically measured using built-in software, and abnormal thinning was displayed on the basis of the CIs of the instrumental normative databases. For cpRNFL analysis on Spectralis, we also computed 99% CIs for the mean thickness of cpRNFL in the 39 normal eyes.

Sensitivity and Specificity

We calculated sensitivity and specificity for detecting abnormal thinning (outside the lower 99% CI limit for the mean of the 39 normal eyes) of each macular layer in at least one 0.5-mm segment of the macula on vertical and horizontal B-scans. We also calculated sensitivity and specificity for the detection of abnormal cpRNFL thinning. In Spectralis, cpRNFL was defined as “abnormal” when the mean thickness of the whole cpRNFL or of at least one sector of the Spectralis sector map was abnormally thin (outside the lower 99% CI

limit for the mean of the instrumental normative database or the 39 normal eyes). In GDx-VCC, cpRNFL was defined as “abnormal” when the mean values of at least one thickness parameters among “NFI,” “TSNIT average,” “superior average,” “inferior average,” or “TSNIT Std. Dev.” was abnormal (outside the lower 99% CI limit for the mean of the instrumental normative database). An additional group of 35 normal eyes were used to calculate specificity.

Statistical Analyses

Differences in the age and spherical equivalent of refractive errors between normal and preperimetric glaucoma groups were compared using unpaired *t*-tests. Differences in gender between the normal and preperimetric glaucoma groups were compared using Fisher’s exact test. McNemar's test was used to compare the sensitivity and specificity for detecting abnormal thinning of macular layer and cpRNFL thickness. Statistical analyses were performed using PASW Statics version 17.0 (SPSS Inc., Chicago, IL). The level of statistical significance was set at $P < 0.05$.

RESULTS

Among the 49 candidate eyes that were selected on the basis of the inclusion/exclusion criteria for the preperimetric group, 37 eyes were judged to have apparent glaucomatous abnormalities, such as neuroretinal rim thinning associated with wedge-shaped localized nerve fiber layer defects (NFLDs; 35 eyes), disc hemorrhages (11 eyes), and both (9 eyes). Evaluation findings of the 3 specialists were unanimous for all the 37 eyes. The evaluation findings of the 3 specialists did not agree in 6 eyes out of the other 10 candidate eyes with preperimetric glaucoma and in 11 of the 44 normal-candidate eyes. The 3

glaucoma specialists made final decisions for these eyes by group discussion. Even after group discussion, the specialists could not reach agreement regarding 2 candidate eyes with preperimetric glaucoma and 2 normal-candidate eyes; these were excluded from analysis. A total of 47 eyes of 47 patients were identified as having preperimetric glaucoma, and 42 eyes from 42 volunteers were identified as normal. After excluding eyes with poor-quality speckle-noise-reduced B-scans, the remaining 37 eyes of 37 patients constituted the preperimetric glaucoma group, and 39 eyes of 39 subjects constituted the normal group for comparison. In the preperimetric glaucoma group, 29 eyes were judged to have neuroretinal rim thinning associated with wedge-shaped localized NFLDs, 9 with disc hemorrhages, and 7 with both. Six eyes were judged to have a vertical cup-to-disc ratio of 0.2 or greater compared to that of the fellow eye; however, all these eyes had disc hemorrhages or neuroretinal rim thinning associated with NFLDs.

The 37 patients with preperimetric glaucoma (24 men and 13 women) ranged in age from 30 to 73 years (mean ± standard deviation [SD], 58.0 ± 9.9 years) and the spherical equivalent of the refractive errors of the 37 eyes with preperimetric glaucoma ranged from -5.5 to +2.0 D (mean ± SD, -1.0 ± 2.3 D). The 39 volunteers (19 men and 20 women) were used to determine abnormal thinning of macular and cpRNFL parameters and to compute 95% and 99% CIs; they ranged in age from 22 to 70 years (mean ± SD, 56.0 ± 13.0 years) and the spherical equivalent of the refractive errors of the 39 normal eyes ranged from -5.5 to +1.0 D (mean ± SD, -1.3 ± 2.1 D). There were no statistically significant differences in gender, age or spherical equivalent of refractive errors between patient and normal groups (P = 0.346, 0.191, and 0.737, respectively).

Another normal group was prepared to calculate specificity; 35 normal eyes from 35 volunteers (18 men and 17 women) were enrolled after 5 eyes were excluded because of disagreement during group

discussion or poor-quality speckle-noise-reduced B-scans. The volunteers' age ranged from 34.2–76.4 years (mean ± SD, 57.4 ± 10.7 years), and the spherical equivalent of the refractive errors ranged from −5.5–2.0 D (-1.4 ± 2.1 D). There were no statistically significant differences with respect to gender, age, or the spherical equivalent of refractive errors between the patients and the other normal groups (P = 0.339, 0.352, and 0.737, respectively).

The disc areas of the study eyes in the preperimetric, first normal, and second normal groups measured by HRT II were 2.43 ± 0.72 mm^2, 2.30 ± 0.53 mm^2, and 2.13 ± 0.77 mm^2, respectively; the ratios of the disc area of the study eyes to that of each fellow eye in the same groups were 1.04 ± 0.15, 0.95 ± 0.11, and 0.99 ± 0.12, respectively.

Visualization of Retinal Layer Boundaries

On speckle-noise-reduced SD-OCT images, the boundary of each retinal layer, including the boundary between the GCL and IPL, was clearly distinguishable (Fig 1). The boundary became more clear as the number of B-scans averaged increased (Fig 2), but there was little difference between averages of 50 and 100 B-scans, so images generated by averaging 50 B-scans were used for this study.

Macular GCL Appearance and Thickness in Normal Eyes

In normal eyes, the GCL in the macula was seen as a well-demarcated hyporeflective layer that had a fairly symmetrical shape across the central fovea (Figs 1 and 2). When the mean macular GCL thickness was compared at every 0.5-mm point from the foveal center, however, the mean macular GCL thickness in the 39 normal eyes appeared to be more symmetrical on either side of the fovea on vertical than on horizontal

B-scans (Fig 3).

On vertical B-scans in normal eyes, as distance from the center of the fovea increased, macular GCL thickness increased rapidly to a peak between 0.73 and 1.40 mm superior to the foveal center (mean ± SD, 0.95 ± 0.18 mm) and from 0.70 to 1.20 mm inferior to the foveal center (mean ± SD, 0.87 ± 0.43 mm) (Fig 3). Peak macular GCL thickness ranged from 43 to 80 μm (mean ± SD, 64.5 ± 7.9 μm) in the superior retinal hemisphere and from 40 to 81 μm (mean ± SD, 66.6 ± 7.4 μm) in the inferior hemisphere. Macular GCL thickness gradually decreased with greater distance from the fovea (Fig 3). On horizontal B-scans, peak macular GCL thickness was located slightly more distant from the foveal center than on vertical B-scans: the nasal peak was 0.9 to 1.9 mm (1.29 ± 0.20 mm) from the center of the fovea and the temporal peak was 0.8 to 1.6 mm (1.24 ± 0.18 mm) from the foveal center (Fig 3). Macular GCL thickness decreased more rapidly from its peak to the periphery on vertical compared to horizontal B-scans.

The superior and inferior macular GCL thicknesses showed statistically significant differences at 1.75, 2.00, 2.25, and 3 mm from the central fovea; the mean differences were 4.7, 6.3, 5.7, and 2.6 μm, respectively, all of which were less than the axial-resolution (7 μm) of Spectralis. The nasal and temporal thickness showed statistically significant differences at 1.00, 1.25, 1.50, 1.75, 2.00, and 2.25 mm from the central fovea; the differences were 5.3, 6.5, 7.5, 8.6, 7.5, 4.2 μm, respectively, and more than the axial-resolution of 7 μm of Spectralis at 1.5, 1.75, and 2.0 mm from the central fovea. Therefore, we compared the nasal-temporal differences with the measurement variability induced by the 2 delineators at 1.5, 1.75, and 2.0 mm from the central fovea. At these distances, the 95% CIs for the mean differences in thickness between 2 delineators with regard to nasal and temporal thickness differences were –4.3 to 2.6 μm, –2.5 to 4.5 μm, and –2.3 to 3.1 μm, and the mean thickness differences between the nasal and temporal

thicknesses were 7.5, 8.6, and 7.5 μm, respectively (Fig 3). Thus, at 1, 1.75, and 2.0 mm from the central fovea, the mean differences between the nasal and temporal thicknesses were outside the limits of 95% CIs for the mean differences between 2 delineators when measuring nasal and temporal thickness.

Mean Macular Retinal Layer Thicknesses on Vertical and Horizontal B-Scans for Preperimetric Glaucoma

When the mean macular GCL thickness was compared between normal eyes and eyes with preperimetric glaucoma at every 0.5-mm point from the foveal center (Fig 4), the mean GCL thickness was significantly thinner in eyes with preperimetric glaucoma than in normal eyes at almost all distances on vertical and horizontal B-scans (inferiorly at 0.5–4 mm, superiorly at 0.5–1.0, and 1.5–4 mm, nasally at 0.5–3.25 mm, and temporally at 0.5–3.75 mm from the foveal center). However, the thickness difference between the groups was greater than the axial-resolution (7 μm) of Spectralis inferiorly (0.75–2.75 mm) and temporally (0.75–2.75 mm) from the foveal center, and superiorly (only at 0.75, 1.0, and 1.75 mm), but nasally not greater at any segment.

When mean thicknesses of each inner retinal layer (RNFL, GCL, and IPL) averaged within defined regions on vertical and horizontal B-scans were compared, eyes with preperimetric glaucoma had significant thinning of the RNFL, the GCL, and RNFL + GCL + IPL (termed the “RGC complex”) compared to normal eyes in the whole region, in both the inferior and superior hemispheres and at all distances from the center of the fovea ($P < 0.0001$ to $P = 0.027$, Table 1). When viewed on horizontal B-scans, eyes with preperimetric glaucoma exhibited significant thinning of the RNFL, GCL, and RGC complex compared to normal eyes in the whole macula, in both inferior and superior hemispheres, and at all distances from the center of the

fovea except for the parafoveal regions for RNFL and the nasal parafoveal region for the RGC complex (P < 0.0001 to P = 0.043, Table 1). Eyes with preperimetric glaucoma did not have significant thinning of the macular IPL in the vertical or horizontal B-scans (Table 1).

Table 1 also shows the number and percentage of eyes with abnormal thinning in each layer at each macular region in eyes with preperimetric glaucoma, which varied according to the layer, region, and vertical/horizontal B-scan. The percentage of eyes with abnormal thinning appears to be larger roughly in the order of GCL > RGC complex > RNFL > IPL on vertical B-scans and GCL = RGC complex > RNFL > IPL on horizontal B-scans. With regard to the macular GCL, the percentage of eyes with abnormal thinning appears to be larger in the order of “inferior” (51.4%) > “superior” (18.9%) = “temporal” (18.9%) > “nasal” (8.1%) hemisphere and “perifovea” (67.6%) > “parafovea” (35.1%) on the vertical B-scans and “perifovea” (16.2%) < “parafovea” (29.7%) on the horizontal B-scans. In addition, the percentage of eyes with abnormal macular GCL thinning appears to be greater in vertical B-scans (10.8%–51.4%) than in horizontal (5.4–21.6%) B-scans.

Figure 5 shows the distribution of percent differences in regional mean thicknesses of the RNFL, GCL, IPL, and RGC complex (RNFL + GCL + IPL) in vertical and horizontal B-scans in eyes with preperimetric glaucoma compared to normal eyes. The mean macular GCL, RNFL, and RGC complex were most severely thinned in the inferior perifovea, where mean macular GCL thickness was less than 70% of normal in 30 (81.1%) of the 37 eyes and less than 50% (49.8% to 21.2%) of normal in 13 (35.1%) of the 37 eyes (Fig 5A,B), the macular RNFL thickness less than 70% of normal in 13 (35.1%) (Fig 5C,D), and the macular RGC complex thickness less than 80% of normal in 14 (37.8%) (Fig 5G,H). In the inferior perifoveal macula, the GCL appeared to be most severely thinned compared to the RNFL and RGC complex (Fig 5).

Sensitivity and Specificity for Detecting Abnormal Thinning

The sensitivity and specificity for detecting abnormal thinning (outside the lower 99% CI limit) in each macular layer thickness on vertical and horizontal B-scans, and in cpRNFL thickness were compared (Table 2). The macular GCL on vertical B-scans exhibited higher sensitivity (81.1%) than the other layers on vertical B-scans (5.4–59.5%, $P = 0.00075$–0.021), the macular GCL (40.5%, $P = 0.00027$) on horizontal B-scans, and the other layers (5.4%–48.6%, $P < 0.00048$–0.004) on horizontal B-scans. The sensitivity for detecting abnormal macular GCL thinning was only slightly higher (83.8%) when eyes with abnormal thinning were counted either on vertical or horizontal B-scan; this sensitivity was higher than that for the RNFL (56.8%, $P = 0.0060$) and RGC complex (70.3%; $P = 0.13$) counted on vertical and horizontal B-scans; the difference regarding the RGC complex was not statistically significant. All the layers on both the vertical and horizontal B-scans exhibited comparable specificity (94.3–100.0%, statistically not different). The sensitivity for detecting abnormal thinning in the macular GCL either on the vertical or horizontal B-scan was significantly higher than that for cpRNFL thickness measured on Spectralis (43.2%, $P = 0.0070$ [calculated using the instrumental normative database]; 54.1%, $P = 0.0010$ [calculated using the data of 39 normal eyes]) and GDx-VCC (24.3%; $P = 0.00040$). The sensitivity for detecting abnormal thinning in the macular RGC complex either on vertical or horizontal B-scan was significantly higher than that for cpRNFL thickness assessed on Spectralis by using the instrumental normative database ($P = 0.006$) and GDx-VCC ($P = 0.00076$); however, it was not significantly different from the cpRNFL thickness assessed on Spectralis by using the data from 39 normal eyes ($P = 0.109$). Specificity was comparable (statistically not different) between the macular parameters (91.4–100.0%) on the vertical or horizontal B-scans as well as cpRNFL

thickness (94.3–97.1%) measured on both instruments.

Case Report

In many eyes with preperimetric glaucoma, local GCL thinning was apparent on visual examination of SD-OCT B-scans, particularly on vertical B-scans (Figs 6–8).

The left eye of a 45-year-old woman was diagnosed as having normal tension glaucoma. The IOP in her left eye was 14–16 mmHg during the first 3 visits. On photographs, the optic disc showed thinning of the inferotemporal neuroretinal rim and a corresponding localized wedge-shaped RNFL defect (Fig 6A,B). The patient had a normal pattern deviation map (Fig 6D) on SAP and normal glaucoma hemifield test, and PSD results. On 9-mm length radial SD-OCT B-scans, local GCL atrophy (Fig 6E,K,L) was evident particularly in the inferior hemisphere when compared to an equivalent area in the superior hemisphere (Fig 6E,I,K). Thinning of the RNFL was associated with the thinning of the GCL. The RNFL in the inferior hemisphere area was borderline thinned (outside the lower 95% CI limit in 39 normal eyes) from –2.0 to –3.0 mm (Fig 7B). The GCL in the inferior hemisphere area was abnormally thinned from –1.5 to –3.0 mm on the vertical B-scan (Fig 7C). Here, the thinning of the macular GCL appeared to be more abrupt and severe. The IPL thickness remained within the 95% normal CI (Fig 7D). Changes in thickness of the RGC complex (Fig 7E) appeared to essentially mirror changes in GCL thickness (Fig 7C). The mean and sectorial cpRNFL thickness were normal (Fig 7G).

DISCUSSION

Glaucoma causes loss of RGCs, which is thought to lead to GCL thinning. To date, however, the GCL has

been difficult to see clearly on single OCT scans, even on ultrahigh-resolution images,[27,28] because of speckle noise in B-scan images.[26,29-32] This study is the first, to our knowledge, to show that the macular GCL in human eyes can be visualized and measured using the speckle-noise-reduction method with SD-OCT B-scan images. We used this method to test the hypotheses that the macular GCL is diminished in preperimetric glaucoma and showed that the macular GCL was diminished on vertical and horizontal speckle-noise-reduced B-scans through the fovea; both the GCL and RNFL were diminished, but the GCL was substantially more diminished.

In normal eyes in our study, on both vertical and horizontal speckle-noise-reduced SD-OCT images, the macular GCL appeared to have the appearance of a fairly symmetric configuration with peak thickness in the central parafoveal region (about 1 mm from the center of the fovea). These results are consistent with reports on RGC densities in enucleated human eyes.[34-36] Mean macular GCL thickness topography curves on vertical and horizontal scans in our study exactly matched fairly symmetric RGC density topography curves shown on vertical and horizontal meridians in enucleated eyes.[36]

In our study, however, the mean macular GCL thicknesses in normal eyes showed differences of more than 7 μm (axial resolution of Spectralis) in the nasal and temporal hemispheres at 1.5−2.0 mm from the central fovea, but did not show differences of more than 7 μm at any distance in the inferior and superior hemispheres. In addition, the nasal and temporal thickness differences of these distances were outside the manual measurement variability limit between delineators. Thus, in the current imaging and measurement settings, the nasal-temporal difference in macular GCL thickness in normal eyes appears to be an actual difference (actual asymmetry) but the superior-inferior thickness difference does not.

In eyes with preperimetric glaucoma, vertical speckle-noise-reduced SD-OCT images revealed

visually apparent thinning of the macular GCL, particularly when compared to an equivalent area in the opposite hemisphere and also when compared to the GCL configuration of normal eyes. The macular GCL thickness measurements confirmed that the GCL was abnormally thin as compared to the normal mean thickness in 30 (81.1%) of our 37 study eyes at least in one 0.5-mm segment. In addition, although the mean macular GCL thickness only exhibited a small difference (81.8% of the normal means), the mean regional macular GCL on vertical B-scans in eyes with preperimetric glaucoma was 57.8% of the normal means in the inferior perifovea; it was thinned in the inferior perifovea to less than 70% of the normal means in 30 (81.1%) of the 37 eyes and to less than 50% of the normal means in 13 (35.1%) eyes. Thus, when we observed macular GCL thinning on vertical B-scans in particular, the macular GCL thinning in the preperimetric glaucoma appeared to occur in local regions; such local thinning would not cause severe thinning in the mean GCL in the macula. These observations of macular GCL thinning in eyes with preperimetric glaucoma appears to be consistent with previous histological studies with enucleated eyes of patients with glaucoma, which suggested that considerable loss of macular RGCs in local regions corresponding to the visual field test points occurs before visual field defects are detected.[1] Thus, speckle-noise-reduction on SD-OCT images may be useful for visualizing and measuring preperimetric RGC damage clinically in patients.

In previous studies that used OCT to study macular RCG structures in eyes with glaucoma, Stratus OCT with originally developed automated measurement software or SD-OCT with commercially available automated measurement software[20-23] was used to measure thickness of the RGC complex of the macula, including the RNFL, GCL, and IPL (termed ganglion cell complex, GCC). These studies consistently showed that the RGC complex was more severely thinned than the total retina in eyes with glaucoma, and of these

studies, 2 that were by Tan et al.[21,22] showed that the RGC complex was significantly thin in eyes with preperimetric glaucoma compared to in normal eyes. However, the configuration of the GCL and its thinning as a result of glaucoma was not clearly visualized in these previous studies. Our study showed that each single layer in the macula was clearly distinguished and measurable, and that the macular GCL and RNFL but not the IPL were significantly thinned in eyes with preperimetric glaucoma compared to normal eyes. Thus, our results were basically consistent with those of these previous studies, but provided more details about damages occurring in the individual layers within the RGC complex in preperimetric glaucoma.

Measuring the RGC complex is advantageous because it can be used to simultaneously assess RGC damage as a single parameter. The feasibility of the automated measurement of the RGC complex with low variability underlies its advantage.[21,34] However, a disadvantage is that the glaucomatous damage of each layer, such as the RNFL, GCL, and IPL, cannot be determined. Because of the anatomical characteristics of the macula, there are differing configurations and symmetry, particularly between the macular RNFL, and GCL—especially the axons of the macular RGCs and the axons of some peripheral RGCs outside the macula merge to pass through the macular area, forming the macular RNFL. Accordingly, morphological changes of the macula caused by the loss of RGCs in glaucoma are not necessarily identical in each layer or region. In fact, our findings suggest that abnormal thinning of each macular layer possibly varies by layer, region, and vertical/horizontal B-scan. Thus, it appears that it is important to know the extent of glaucomatous damage to each layer, such as GCL and RNFL. Our knowledge of preperimetric glaucomatous RGC loss is based on previously reported histopathological studies of the retina and optic nerve using enucleated patients eyes.[1,2] It is difficult to use such histopathological methods for a large scale clinical investigation. Our findings indicate that although we cannot observe the cell bodies or axons of

individual RGCs, speckle-noise-reduction in SD-OCT imaging provides a unique opportunity for non-invasively observing and assessing damages of RGC somas, and axons as abnormal thinning of the macular GCL and RNFL, which will be able to be used for future clinical research in a large scale.

In our study, we could not fully assess the glaucoma discriminating ability of macular GCL because automated measurement of each layer was not available in the instrument used, and because our analysis did not include the entire macular area. Although macular GCL exhibited highest sensitivity for detecting preperimetric glaucomatous abnormalities, it remains unclear whether the measurement of a single GCL layer can discriminate glaucoma better than the measurement of the RGC complex. In our preliminary experiments conducted by using original CI maps on the basis of 39 normal eyes, the macular GCL either exhibited higher sensitivity than the other macular layers including the macular RGC complex, although the difference regarding the macular RGC complex was not statistically supported in our subjects. Macular GCL exhibited higher sensitivity than cpRNFL thickness as assessed on Spectralis by using the same normal data, whereas we did not detect significantly higher sensitivity in the macular RGC complex compared to the cpRNFL thickness assessed by using the same normal data. It was previously shown that selective measurement of the macular RGC complex has better ability to discriminate glaucoma than measurement of the total retinal thickness in the macula.[20-25,34] This is attributed to the fact that the total retina includes the outer retinal layers that are minimally diminished in glaucoma (if any), whereas the macular RGC complex does not.[22] Similarly, inclusion of macular IPL, which did not exhibit significant thinning on vertical or horizontal B-scans in our study, potentially decreases the sensitivity of the macular RGC complex for detecting glaucomatous changes. Thus, although our study was performed manually, the results encourage the development of an automated segmentation algorithm for dense B-scans over the whole macula to

determine whether selective measurement of GCL may have comparable or better glaucoma-discriminating ability than known OCT parameters such as cpRNFL and RGC complex.

The results of this study may raise the question, "How can SAP results remain normal after the GCL has become abnormally thin?" One possible explanation is that there may be sufficient redundancy in the visual system of RGCs in the normal macula whose function, at least as measured by SAP, remains normal despite considerable loss of RGCs.[1-3] Another possible explanation is that there is some loss of function, but it is not identified by the SAP 24-2 program because of the relatively low spatial resolution of test points; test points are about 5 degrees apart, representing a distance of almost 1.25 mm on the retina; hence, thinning of the macular GCL limited to areas between the SAP test points might not be detected by SAP. Further studies using short-wavelength automated perimetry, frequency-doubling technology perimetry, and 10-2 SAP may clarify this question.

A limitation of this pilot study is that thickness measurements were performed only on vertical and horizontal B-scan images, which do not show the entire macula; these images show only certain aspects of macular GCL morphology. Despite this limitation, our study demonstrated that speckle-noise-reduction in SD-OCT imaging can be used to clinically visualize and measure the macular GCL in human eyes. On the speckle-noise-reduced SD-OCT images, the macular GCL in eyes with preperimetric glaucoma showed visually apparent and quantitatively abnormal thinning as compared to normal eyes. Macular GCL imaging using speckle-noise-reduction of SD-OCT B-scans may be potentially useful for facilitating understanding of glaucomatous structural damages of the macula.

REFERENCES

1. Quigley HA, Dunkelberger GR, Green WR. Retinal ganglion cell atrophy correlated with automated perimetry in human eyes with glaucoma. Am J Ophthalmol 1989;107:453-64.
2. Kerrigan-Baumrind LA, Quigley HA, Pease ME, et al. Number of ganglion cells in glaucoma eyes compared with threshold visual field tests in the same persons. Invest Ophthalmol Vis Sci 2000;41:741-8.
3. Harwerth RS, Carter-Dawson L, Shen F, et al. Ganglion cell losses underlying visual field defects from experimental glaucoma. Invest Ophthalmol Vis Sci 1999 ;40:2242-50.
4. Hoyt WF, Newman NM. The earliest observable defect in glaucoma? Lancet 1972;1:692-3.
5. Sommer A, Pollack I, Maumenee AE. Optic disc parameters and onset of glaucomatous field loss. I. Methods and progressive changes in disc morphology. Arch Ophthalmol 1979;97:1444-8.
6. Funk J. Early detection of glaucoma by longitudinal monitoring of the optic disc structure. Graefes Arch Clin Exp Ophthalmol 1991;229:57-61.
7. Sommer A, Katz J, Quigley HA, et al. Clinically detectable nerve fiber atrophy precedes the onset of glaucomatous field loss. Arch Ophthalmol 1991;109:77-83.
8. Motolko M, Drance SM. Features of the optic disc in preglaucomatous eyes. Arch Ophthalmol 1981;99:1992-4.
9. Kass MA, Heuer DK, Higginbotham EJ, et al. The Ocular Hypertension Treatment Study: A randomized trial determines that topical ocular hypotensive medication delays or prevents the onset of primary open-angle glaucoma. Arch Ophthalmol 2002;120:701-13.
10. Zeimer R, Asrani S, Zou S, et al. Quantitative detection of glaucomatous damage at the posterior pole by

retinal thickness mapping. A pilot study. Ophthalmology 1998;105:224-31.

11. Giovannini A, Amato G, Mariotti C. The macular thickness and volume in glaucoma: an analysis in normal and glaucomatous eyes using OCT. Acta Ophthalmol Scand Suppl 2002;236:34-6.
12. Guedes V, Schuman JS, Hertzmark E, et al. Optical coherence tomography measurement of macular and nerve fiber layer thickness in normal and glaucomatous human eyes. Ophthalmology 2003;110:177-89.
13. Lederer DE, Schuman JS, Hertzmark E, et al. Analysis of macular volume in normal and glaucomatous eyes using optical coherence tomography. Am J Ophthalmol 2003;135:838-43.
14. Greenfield DS, Bagga H, Knighton RW. Macular thickness changes in glaucomatous optic neuropathy detected using optical coherence tomography. Arch Ophthalmol 2003;121:41-6.
15. Wollstein G, Schuman JS, Price LL, et al. Optical coherence tomography (OCT) macular and peripapillary retinal nerve fiber layer measurements and automated visual fields. Am J Ophthalmol 2004;138:218-25.
16. Wollstein G, Ishikawa H, Wang J, et al. Comparison of three optical coherence tomography scanning areas for detection of glaucomatous damage. Am J Ophthalmol 2005;139:39-43.
17. Medeiros FA, Zangwill LM, Bowd C, et al. Evaluation of retinal nerve fiber layer, optic nerve head, and macular thickness measurements for glaucoma detection using optical coherence tomography. Am J Ophthalmol 2005;139:44–55.
18. Leung CK, Chan WM, Yung WH, et al. Comparison of macular and peripapillary measurements for the detection of glaucoma: An optical coherence tomography study. Ophthalmology. 2005;112:391-400.
19. Ojima T, Tanabe T, Hangai M, et al. Measurement of retinal nerve fiber layer thickness and macular

volume for glaucoma detection using optical coherence tomography. Jpn J Ophthalmol 2007;51:197-203.

20. Ishikawa H, Stein DM, Wollstein G, et al. Macular segmentation with optical coherence tomography. Invest Ophthalmol Vis Sci 2005;46:2012-7.

21. Tan O, Li G, Lu AT, et al. Mapping of macular substructures with optical coherence tomography for glaucoma diagnosis. Ophthalmology 2008;115:949-56.

22. Tan O, Chopra V, Lu AT, et al. Detection of macular ganglion cell loss in glaucoma by Fourier-domain optical coherence tomography. Ophthalmology 2009;116:2305-14.

23. Seong M, Sung KR, Choi EH, et al. Macular and peripapillary retinal nerve fiber layer measurements by spectral domain optical coherence tomography in normal-tension glaucoma. Invest Ophthalmol Vis Sci 2010;51:1446-52.

24. Kotera Y, Hangai M, Hirose F, Mori S, Yoshimura N. Three-dimensional imaging of macular inner structures in glaucoma by using spectral-domain optical coherence tomography. Invest Ophthalmol Vis Sci. In press.

25. Sakamoto A, Hangai M, Nukada M, et al. Three-dimensional imaging of the macular retinal nerve fiber layer in glaucoma with spectral-domain optical coherence tomography. Invest Ophthalmol Vis Sci 2010;51:5062-70.

26. Hangai M, Yamamoto M, Sakamoto A, Yoshimura N. Ultrahigh-resolution versus speckle noise-reduction in spectral-domain optical coherence tomography. Opt Express 2009;17:4221-35.

27. Wollstein G, Paunescu LA, Ko TH, et al. Ultrahigh-resolution optical coherence tomography in glaucoma. Ophthalmology 2005;112:229-37.

28. Mumcuoglu T, Wollstein G, Wojtkowski M, et al. Improved visualization of glaucomatous retinal damage using high-speed ultrahigh-resolution optical coherence tomography. Ophthalmology 2008;115:782-9.

29. Schmitt JM, Xiang SH, Yung KM. Speckles in optical coherence tomography. J Biomed Optics 1999;4:95-105.

30. Sander B, Larsen M, Thrane L, et al. Enhanced optical coherence tomography imaging by multiple scan averaging. Br J Ophthalmol 2005 ;89:207-12.

31. Sakamoto A, Hangai M, Yoshimura N. Spectral-domain optical coherence tomography with multiple B-scan averaging for enhanced imaging of retinal diseases. Ophthalmology 2008;115:1071-8.

32. Byeon SH, Chu YK, Lee H, et al. Foveal ganglion cell layer damage in ischemic diabetic maculopathy. Correlation of optical coherence tomographic and anatomic changes. Ophthalmology 2009;116:1949-59.

33. Ooto S, Hangai M, Sakamoto A, et al. Three-dimensional profile of macular retinal thickness in normal Japanese eyes. Invest Ophthalmol Vis Sci 2010;51:465-73.

34. Mori S, Hangai M, Sakamoto A, Yoshimura N. Spectral-domain optical coherence tomography measurement of macular volume for diagnosing glaucoma. J Glaucoma. 2010;19:528-34.

35. Van Buren JM. The Retinal Ganglion Cell Layer. Springfield, IL: Charles C. Thomas; 1963.

36. Wassle H, Grunert U, Rohrenbeck J, Boycott BB. Cortical magnification factor and the ganglion cell density of the primate retina. Nature 1989;341:643-6.

37. Curcio CA, Allen KA. Topography of ganglion cells in human retina. J Comp Neurol 1990;300:5-25.

Re-revised Table 1 Mean Macular Retinal Layer Thicknesses Profile Measured on Vertical and Horizontal Scans in Eyes with and without Glaucoma

	Retinal Layer	Location of Measurement		Normal Eyes (n = 39)		Preperimetric Glaucoma Eyes (n = 37)		N (%)*	*P* Value†
				Mean (SD)	Range	Mean (SD)	Range		
Vertical Scan	GCL	Macula		34.6 (2.3)	28.1-41.8	28.3 (4.8)	18.8-37.7	12 (32.4)	< 0.0001
		Hemisphere	S	35.8 (3.0)	30.0-42.5	31.6 (6.5)	11.0-41.0	7 (18.9)	0.001
			I	33.5 (3.1)	26.0-38.0	25.0 (5.2)	13.2-39.7	19 (51.4)	< 0.0001
		Parafovea	S	55.5 (5.1)	45.5-66.5	50.6 (10.5)	17.5-66.5	4 (10.8)	0.017
			I	56.1 (5.1)	44.5-66.0	45.9 (10.0)	23.5-63.5	9 (24.3)	< 0.0001
		Perifovea	S	29.9 (3.9)	20.7-40.7	25.4 (7.1)	7.7-39.0	6 (16.2)	0.003
			I	26.8 (2.7)	23.3-37.7	15.5 (5.3)	7.0-30.7	19 (51.4)	< 0.0001
	RNFL	Macula		32.7 (3.1)	26.8-37.2	28.1 (4.0)	18.8-35.4	5 (13.5)	< 0.0001
		Hemisphere	S	32.8 (3.7)	25.5-40.5	28.9 (5.0)	19.5-40.8	5 (13.5)	< 0.0001
			I	32.7 (3.0)	26.5-38.8	27.2 (4.5)	15.8-38.3	12 (32.4)	< 0.0001
		Parafovea	S	28.7 (4.0)	22.0-39.0	26.6 (4.3)	19.0-37.0	0	0.027
			I	28.9 (3.1)	20.5-37.5	26.6 (3.8)	19.0-36.5	3 (8.1)	0.004
		Perifovea	S	43.6 (5.4)	34.3-54.0	37.5 (7.2)	23.0-54.3	4 (10.8)	< 0.0001
			I	43.3 (4.8)	34.3-53.0	33.9 (7.2)	17.3-51.3	13 (42.6)	< 0.0001
	IPL	Macula		29.9 (3.2)	23.5-36.4	32.7 (3.8)	23.6-40.3	0	0.033
		Hemisphere	S	30.4 (3.5)	23.8-38.2	31.8 (4.1)	23.3-38.2	0	0.154
			I	29.4 (3.4)	23.1-36.2	32.3 (4.1)	23.8-43.7	0	0.012
		Parafovea	S	34.8 (4.3)	26.5-42.0	36.8 (4.1)	27.0-45.0	0	0.049
			I	34.2 (4.8)	26.0-45.0	36.6 (4.6)	26.5-53.5	0	0.117
		Perifovea	S	33.4 (4.7)	24.3-43.7	35.0 (5.9)	26.3-44.3	0	0.243
			I	31.5 (4.0)	23.3-36.3	35.9 (5.6)	24.3-53.0	0	0.003
	RGC complex	Macula		97.5 (5.6)	81.2-107.7	88.7 (9.0)	69.8-104.2	11 (29.7)	< 0.0001
		Hemisphere	S	98.9 (5.9)	81.0-111.5	92.1 (10.8)	68.1-105.2	9 (24.3)	0.001
			I	96.2 (6.1)	81.3-108.2	85.4 (10.5)	66.3-110.3	14 (37.8)	< 0.0001
		Parafovea	S	119.0 (7.3)	94.5-131.5	113.7 (12.5)	81.0-127.0	6 (16.2)	0.021
			I	119.1 (8.2)	99.5-139.5	109.6 (12.4)	80.5-132.0	8 (21.6)	< 0.0001
		Perifovea	S	106.7 (8.5)	92.6-123.0	97.7 (13.2)	73.7-129.3	9 (24.3)	0.001
			I	100.9 (8.1)	86.0-113.7	86.7 (13.9)	62.7-125.7	12 (32.4)	< 0.0001
Horizontal Scan	GCL	Macula		39.7 (4.8)	28.3-47.9	34.3 (5.6)	14.6-43.3	2 (5.4)	< 0.0001
		Hemisphere	N	41.7 (5.6)	28.5-51.5	37.8 (7.0)	11.5-46.5	3 (8.1)	0.010
			T	37.7 (4.4)	28.2-44.3	30.7 (5.9)	17.7-40.3	7 (18.9)	< 0.0001
		Parafovea	N	55.5 (7.3)	30.5-69.0	51.1 (9.5)	12.5-62.5	3 (8.1)	0.027
			T	50.3 (6.2)	36.5-58.5	42.2 (8.5)	17.0-56.5	8 (21.6)	< 0.0001
		Perifovea	N	42.6 (7.2)	29.0-58.0	37.9 (8.0)	13.0-51.3	2 (5.4)	0.008
			T	38.3 (5.2)	26.3-46.7	30.2 (6.8)	16.3-47.7	4 (10.8)	< 0.0001

RNFL	Macula		22.1 (1.9)	17.1-25.4	20.8 (1.7)	18.2-25.6	0	0.002
	Hemisphere	N	29.9 (3.2)	22.7-36.5	28.3 (3.2)	21.8-34.2	0	0.037
		T	14.3 (1.6)	11.5-17.5	13.8 (1.8)	10.7-17.5	0	0.012
	Parafovea	N	20.4 (2.3)	13.0-23.9	19.7 (2.4)	14.1-23.9	0	0.165
		T	15.4 (2.0)	12.5-19.6	14.8 (1.9)	11.0-18.5	0	0.196
	Perifovea	N	44.0 (5.3)	34.7-56.7	41.5 (5.5)	28.7-50.3	2 (5.4)	0.043
		T	16.1 (2.2)	12.0-21.3	14.6 (2.8)	9.7-20.3	1 (2.7)	0.009
IPL	Macula		30.0 (2.6)	25.1-33.8	30.4 (2.3)	25.8-34.4	0	0.493
	Hemisphere	N	30.4 (2.9)	23.5-35.7	31.1 (2.8)	25.3-36.2	0	0.249
		T	29.6 (2.8)	24.5-34.5	29.7 (2.4)	23.5-34.0	0	0.996
	Parafovea	N	33.1 (3.3)	25.2-38.1	34.5 (3.7)	26.0-41.5	0	0.099
		T	32.2 (3.0)	25.6-37.7	33.2 (3.1)	26.5-41.1	0	0.184
	Perifovea	N	34.9 (4.1)	26.7-43.7	35.7 (3.1)	30.0-41.7	0	0.326
		T	34.4 (4.3)	25.3-41.7	33.6 (3.1)	26.3-38.2	0	0.354
RGC complex	Macula		91.8 (5.3)	78.3-100.8	85.7 (7.2)	65.4-98.9	8 (21.6)	< 0.0001
	Hemisphere	N	101.9 (7.1)	83.4-112.5	97.2 (10.0)	67.0-115.5	5 (13.5)	0.022
		T	81.8 (4.4)	73.0-90.7	74.1 (7.2)	56.3-96.3	7 (18.9)	< 0.0001
	Parafovea	N	109.1 (9.2)	80.5-125.4	105.9 (11.5)	70.0-122.5	2 (5.4)	0.182
		T	98.1 (7.3)	79.3-112.5	90.7 (10.1)	66.0-124.5	4 (10.8)	0.001
	Perifovea	N	121.5 (9.0)	99.7-136.3	114.4 (12.6)	79.0-137.3	4 (10.8)	0.007
		T	89.0 (5.6)	78.7-100.0	78.8 (8.7)	57.3-97.7	5 (13.5)	< 0.0001

* Number and percent of eyes with abnormal thinning in each macular layer at each macular region in eyes with preperimetric glaucoma. Macular thickness at each region were defined as “abnormal” when the mean thickness was abnormally thin (outside the lower 99% confidential interval confidential limit in the normal eyes).

† Unpaired *t*-test

GCL = ganglion cell layer; I = Inferior; IPL = inner plexiform layer; RGC = retinal ganglion cell; RGC complex = RNFL + GCL + IPL; RNFL = retinal nerve fiber layer; S = Superior; SD = 1 standard deviation

Table 2. Sensitivity and Specificity for Detecting Abnormal Thinning of Macular Layer Structures and the Circumpapillary Retinal Nerve Fiber Layer

			No. of Eyes with Abnormal Thinning in PPG (Sensitivity [%]) n = 37	No. of Eyes with Abnormal Thinning in Normal Eyes (Specificity [%]) n = 35
Macular Thickness* (Normal eye data of this study)	GCL	Vertical	30 (81.1)	0 (100.0)
		Horizontal	15 (40.5)	1 (97.1)
		V or H	31 (83.8)	1 (97.1)
	RNFL	Vertical	18 (48.6)	1 (97.1)
		Horizontal	8 (21.6)	2 (94.3)
		V or H	21 (56.8)	3 (91.4)
	IPL	Vertical	2 (5.4)	0 (100.0)
		Horizontal	2 (5.4)	0 (100.0)
		V or H	4 (10.8)	0 (100.0)
	RGC complex	Vertical	22 (59.5)	0 (100.0)
		Horizontal	18 (48.6)	2 (94.3)
		V or H	26 (70.3)	2 (94.3)
cpRNFL (Spectralis)†	Instrumental normative database		16 (43.2)	2 (94.3)
	Normal eye data of this study		20 (54.1)	2 (94.3)
cpRNFL (GDx-VCC)‡	Instrumental Normative database		9 (24.3)	1 (97.1)

*Macular thickness parameters were defined as “abnormal” when the mean thickness was abnormally thin (outside the lower 99% confidential interval [CI] limit in our normal eyes) in at least one 0.5-mm segment of the macula along vertical or horizontal scan.

†cpRNFL on Spectralis was defined as “abnormal” when the mean thickness of the whole cpRNFL or at least one sector of cpRNFL was abnormally thin (outside the lower 99% CI limit for the mean of the instrumental normative database or the normal eyes).

‡cpRNFL on GDx-VCC was defined as “abnormal” when the mean values of at least one thickness parameters among “NFI,” “TSNIT average,” “superior average,” “inferior average,” or “TSNIT Std. Dev.” were abnormal (outside the lower 99% CI limit for the mean of the instrumental normative database).

cpRNFL = circumpapillary retinal nerve fiber layer; GCL = ganglion cell layer; H = horizontal; IPL = inner plexiform layer; PPG = preperimetric glaucoma; RGC = retinal ganglion cell; RGC complex = RNFL + GCL + IPL; V = vertical; VCC = variable corneal compensation

Figure Legends

Figure 1. Speckle-noise-reduced spectral-domain optical coherence tomography (SD-OCT) B-scans through the central fovea in a normal eye. **A, B,** Horizontal **(A)** and vertical **(B)** 9-mm scans show clearly distinguishable layers. **C,** Magnified view of inferior macular region in **(B)** showing ganglion cell layer (GCL), retinal nerve fiber layer (RNFL), and inner plexiform layer (IPL). The double-headed arrows indicate various distances from the central fovea (zero); the segment from 0 to 0.5 mm is considered to be within the fovea, 0.5 to 1.5 mm is considered the parafoveal region, and 1.5 to 3.0 mm is considered the perifoveal segment. The shape of the GCL and IPL appears vertically and horizontally symmetrical and that of RNFL appears to be only vertically symmetrical.

Figure 2. Images showing effects of speckle-noise-reduction by multiple B-scan averaging of spectral-domain optical coherence tomography (SD-OCT) B-scans in a normal eye. **A, B**, Single B-scan image. **C,D,** Average of 10 B-scans at the same location. **E,F,** Average of 50 B-scans at the same location. **B,D,F,** Magnified (4X) views of areas outlined by red dashed lines in **A, C,** and **E** show that averaging more scans results in greater reduction in speckle noise and increasing clarification of the boundaries between the retinal nerve fiber layer (RNFL), ganglion cell layer (GCL), and inner plexiform layer (IPL).

Figure 3. Mean macular ganglion cell layer (GCL) thickness in normal eyes as a function of distance from the central fovea along the horizontal **(A−C)** and vertical **(D−F)** ocular meridians. Mean macular GCL thicknesses in the nasal **(A)**, temporal **(B)**, superior **(D)**, and inferior **(E)** hemispheres as measured by 2 independent delineators were superimposed. Mean arbitrated macular GCL thickness of the nasal−temporal

(C), and superior−inferior **(F)** hemispheres were superimposed. Arbitration was performed by group review and discussion among the 2 delineators and a third observer. In the horizontal meridian **(A),** the gap in the nasal curve 3.5 mm from the center of the fovea represents the site of the optic nerve head. *$P < 0.0001$; **$P < 0.001$; ***$P < 0.05$

Figure 4. Superimposed graphs for the mean thickness of the macular ganglion cell layer (GCL); data for eyes with preperimetric glaucoma was superimposed on that for normal eyes as a function of distance from the central fovea along the vertical and horizontal ocular meridians. The mean thickness of the macular GCL in the superior **(A)**, inferior **(B)**, nasal (C), and temporal (D) hemispheres arbitrated by group review and discussion among the 2 delineators and a third observer are plotted. *$P < 0.0001$; **$P < 0.001$; ***$P < 0.05$

Figure 5. Histograms showing percent thickness of the macular ganglion cell layer (GCL) (**A,B**), macular retinal nerve fiber layer (RNFL) (**C,D**), macular inner plexiform layer (IPL) (**E,F**), and retinal ganglion cell complex (RGC complex = RNFL+GCL+IPL) in the macula (**G,H**) on vertical (**A,C,E,G**) and horizontal (**B,D,F,H**) 9-mm speckle-noise-reduced spectral-domain optical coherence tomography (SD-OCT) B-scans in eyes with preperimetric glaucoma (n=37) compared to mean thickness of these layers in normal eyes (n=39). **A-1, C-1, E-1, G-1,** Results for the macular, inferior macular, and superior macular regions. **A-2, C-2, E-2, F-2,** Results for the inferior and superior perifoveal regions (1.5–3.0 mm from the center of the fovea) and for the inferior and superior parafoveal regions (0.5–1.5 mm from the center of the fovea). **B-1, D-1, F-1, H-1,** Results for the macular, nasal macular, and temporal macular regions. **B-2, D-2, F-2, H-2,** Results for the nasal and temporal perifoveal and parafoveal regions.

Figure 6. Macular ganglion cell layer (GCL) thinning visible on radial speckle-noise-reduced spectral-domain optical coherence tomography (SD-OCT). The patient was a 45-year-old woman and intraocular pressure in the left eye was 14–16 mmHg without glaucoma medication. On color disc (**A**) and fundus (**B**) photographs of this patient's left eye, localized thinning of the neuroretinal rim of the optic nerve head (white arrow) and wedge-shaped retinal nerve fiber layer (RNFL) defects (white arrowheads) are visible. **C,** This infrared image of the right eye shows the directions of radial 9-mm speckle-noise-reduced SD-OCT B-scans of the right eye shown in **E-L**. The red portions of the yellow arrows indicate where the ganglion cell layer (GCL) appears thinned on the SD-OCT images (inferior hemisphere) and blue portions of the arrows indicate the equivalent regions in the superior hemisphere. **D,** Humphrey 24-2 SITA standard pattern deviation map. **E,** Vertical SD-OCT B-scans through the fovea. Localized GCL thinning (red double-headed arrows) is evident in the inferior hemisphere (left side of the image) but not in the superior hemisphere (blue double-headed arrow indicates the comparable distance from the central fovea). **F, G,** Magnified (2X) view of areas outlined by red dashed lines in **E**. The red dashed lines in G represent the boundaries of the macular GCL. RNFL = retinal nerve fiber layer; IPL = inner plexiform layer. Thinning of the RNFL is associated with GCL atrophy. The inner plexiform layer (IPL) appears to be elevated where the GCL is thinned, but it does not appear atrophic. **H-L,** Radial SD-OCT B-scans centered on the central fovea. The GCL is noticeably thinned in a segment of the inferior hemisphere **(K,L;** red double-headed arrows**)** compared to the equivalent area of the superior hemisphere **(I,H;** blue double-headed arrows).

Figure 7. Manual delineation of retinal layer boundaries **(A)** and macular retinal layer thickness measurements calculated by SD-OCT software by using vertical B-scans through the central fovea of the right eye (shown in Figure 6). **A,** Red boundary lines delineate the retinal nerve fiber layer (RNFL), ganglion cell layer (GCL), and inner plexiform layer (IPL) and were used for calculations of RNFL, GCL, and IPL thickness at various distances from the central fovea to the periphery. **B-E,** Thickness curves (black lines) for the RNFL, GCL, IPL, and the retinal ganglion cell complex (RGC complex = RNFL+GCL+IPL) in this eye, which were generated from thickness calculations at various distances from the central fovea (negative numbers on the X-axis represent distances from the central fovea in the inferior hemisphere; positive numbers represent distances in the superior hemisphere). Colored graphs were drawn using the mean (green line) and confidence intervals of mean thicknesses measured in 39 normal Japanese eyes that were examined at Kyoto University Hospital. The sector maps in the right column of **(B)–(E)** indicate the mean thickness within every 0.5-mm segment from the central fovea. The red double-headed arrows indicate the thinning of each layer as compared to its mean thickness in normal eyes. Red horizontal lines indicate equivalent points in the superior and inferior hemispheres. The GCL **(C)** is greatly thinned in the inferior hemisphere as compared to the mean thickness at an equivalent location in the superior hemisphere and as compared to the mean thickness in normal eyes in this study (green line). Compared to normal eyes, the GCL in this eye is abnormally thinned in 3 inferior segments from 1.5 to 3.0 mm. The RNFL thinning in this eye (black line in **B**) appears to be milder compared to GCL thinning and borderline thinning is observed in 2 inferior segments from 2.0 to 3.0 mm. The IPL thickness is within normal limits in all segments. Abnormal thinning of the RGC complex **(E)** was detected in the 3 inferior segments from 1.5 to 3.0 mm. **F,G,** Automated measurement of circumpapillary RNFL (cpRNFL) thickness by using built-in software. **F,** Red

boundary lines delineate the cpRNFL. **G,** The cpRNFL thickness map in the left column shows the mean (green line) and confidence intervals of mean thickness in the instrumental normative database. The sector map in the right column indicates the mean cpRNFL thickness within each sector and the whole. The color coding is as follows: purple, abnormal thickening (values higher than the upper 99% confidence interval [CI] limit for the mean in the 39 normal eyes); red, abnormal thinning (values lower than the lower 99% CI limit for the mean in normal eyes); blue, borderline thickened (values between the upper 95% and upper 99% CI limit for the mean in normal eyes); yellow, borderline thinned (values between the lower 95% and lower 99% CI limit for the mean for normal eyes); and green, within normal limits (values between the upper and lower 95% CI limit for the mean in the 39 normal eyes). The Y-axis indicates thickness values (μm).

Figure 8. Photographs, vertical 9-mm speckle-noise-reduced spectral-domain optical coherence tomography (SD-OCT) B-scan images, and macular ganglion cell layer (GCL) thickness curves based on manual SD-OCT measurements of 2 eyes with preperimetric glaucoma. **A–C,** Images of a normal eye, **D–O,** Images of eyes with preperimetric glaucoma. **A,D,J,** Color disc photographs. **G,M,** Color fundus photographs. White arrows indicate neuroretinal rim thinning in the optic nerve head, and white arrowheads indicate wedge-shaped localized retinal nerve fiber layer defects. **B,C,E,F,H,K,L,N,** Vertical SD-OCT B-scans. **C, F, H, L, N,** Magnified (2X) view of areas outlined by red dashed lines in **(B), (E)** and **(K)**. The red dashed lines in **H and N** represent the boundaries of the macular GCL. Localized thinning of the macular GCL at various distances from the central fovea is evident in the inferior hemisphere (red arrows), compared to an equivalent area in the superior hemisphere (blue arrows) and to an equivalent area in a normal macular GCL. **I, O**, Graphs of mean thickness curves of the GCL on vertical scans of 2 eyes with

preperimetric glaucoma. The X-axis indicates distances (mm) from the central fovea in the inferior hemisphere (left side; negative numbers) and superior hemisphere (right side; positive numbers). The Y-axis indicates GCL thickness (μm). Color-coded curves are based on measurements obtained for 39 normal Japanese eyes examined at Kyoto University Hospital. The sector maps in the right column of **(I)** and **(O)** indicate the mean thickness every 0.5 mm from the central fovea. The color coding is as follows: purple = abnormal thickening (values above the upper 99% confidence interval [CI] limit for the mean in normal eyes); red = abnormal thinning (values lower than the lower 99% CI limit for the mean in normal eyes); blue = borderline thickening (values between the upper 95% and upper 99% CI limit for the mean in normal eyes); yellow = borderline thinning (values between the lower 95% and lower 99% CI limit for the mean in normal eyes); and green = within normal limits (values between the upper 95% and lower 95% CI limit for the mean in normal eyes). The macular GCL was abnormally thin in the inferior hemisphere in both eyes in some segments where the GCL thickness (black line) decreased as compared to that in the superior hemisphere (red horizontal line) and as compared to the mean in normal eyes (green line); red double-headed arrows indicate this difference.

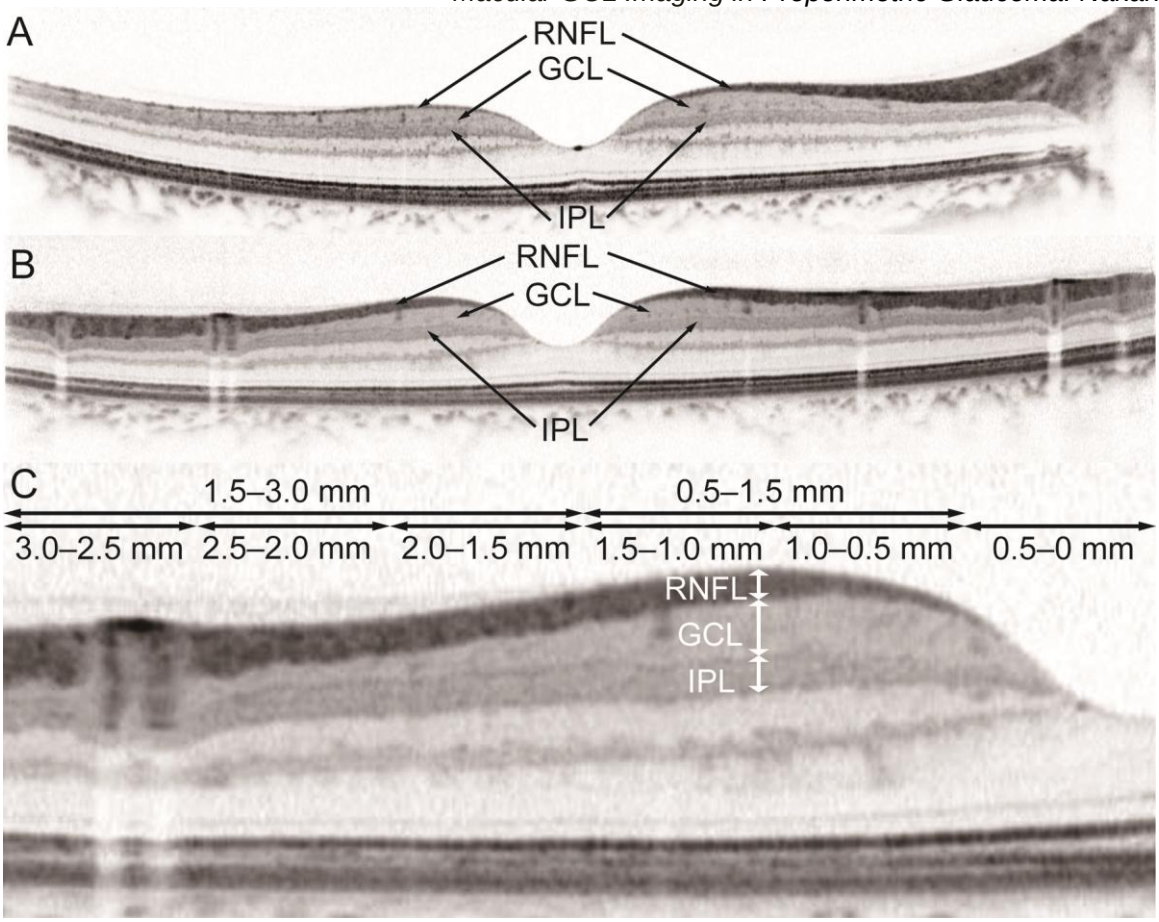
A
RNFL
GCL
IPL
B
RNFL
GCL
IPL
C
1.5–3.0 mm
0.5–1.5 mm
3.0–2.5 mm
2.5–2.0 mm
2.0–1.5 mm
1.5–1.0 mm
1.0–0.5 mm
0.5–0 mm
RNFL
GCL
IPL

Figure 1

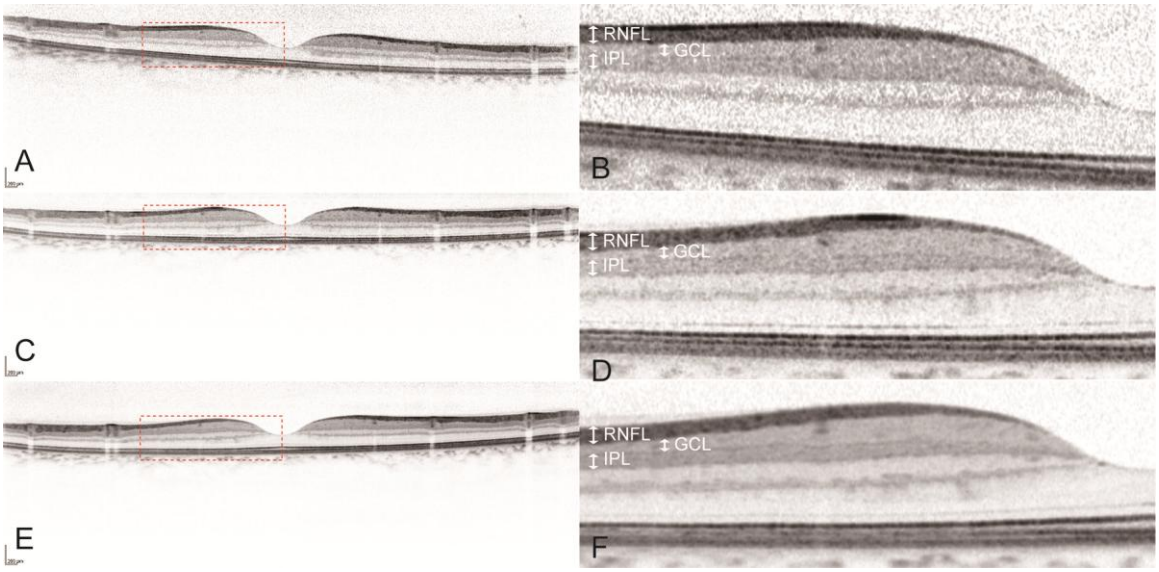

Figure 2

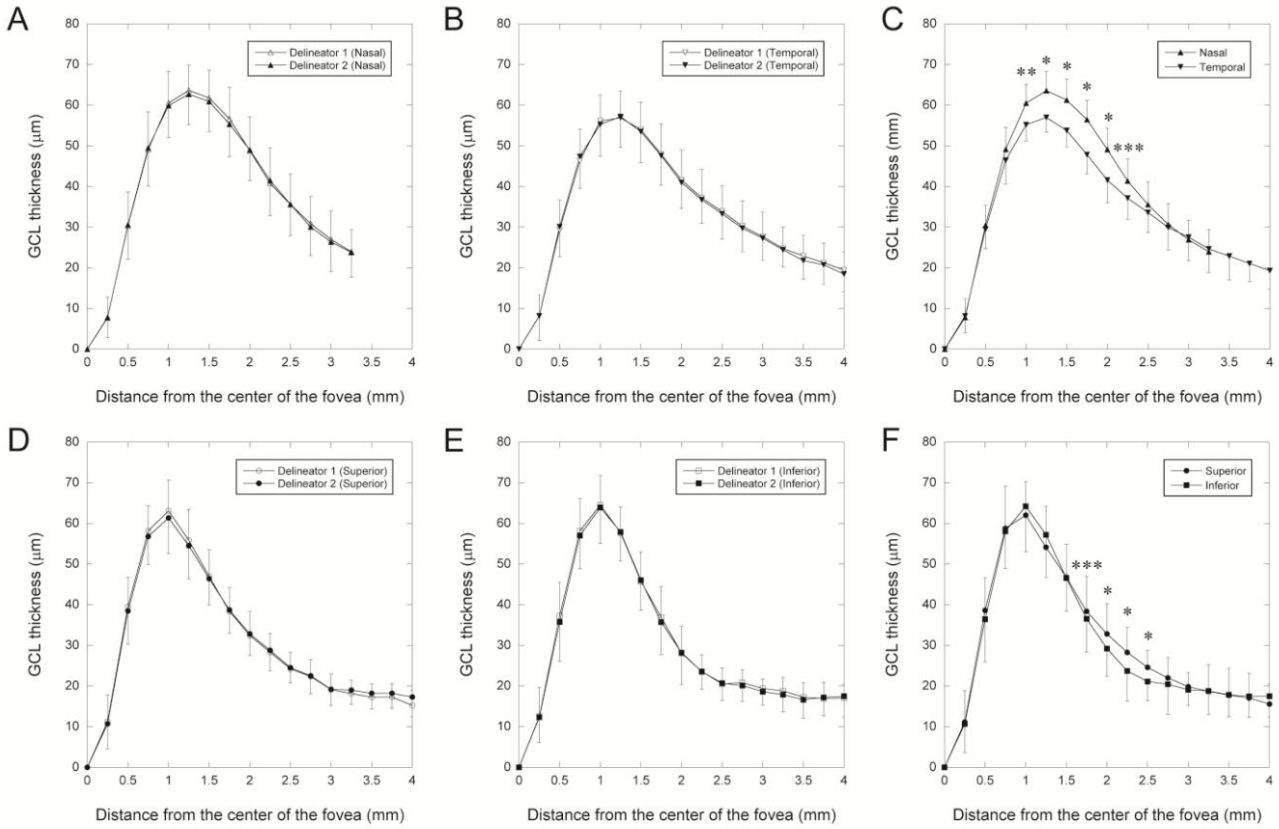
A
Delineator 1 (Nasal)
Delineator 2 (Nasal)
B
Delineator 1 (Temporal)
Delineator 2 (Temporal)
C
Nasal
Temporal
D
Delineator 1 (Superior)
Delineator 2 (Superior)
E
Delineator 1 (Inferior)
Delineator 2 (Inferior)
F
Superior
Inferior
GCL thickness (μm)
GCL thickness (mm)
Distance from the center of the fovea (mm)

Figure 3

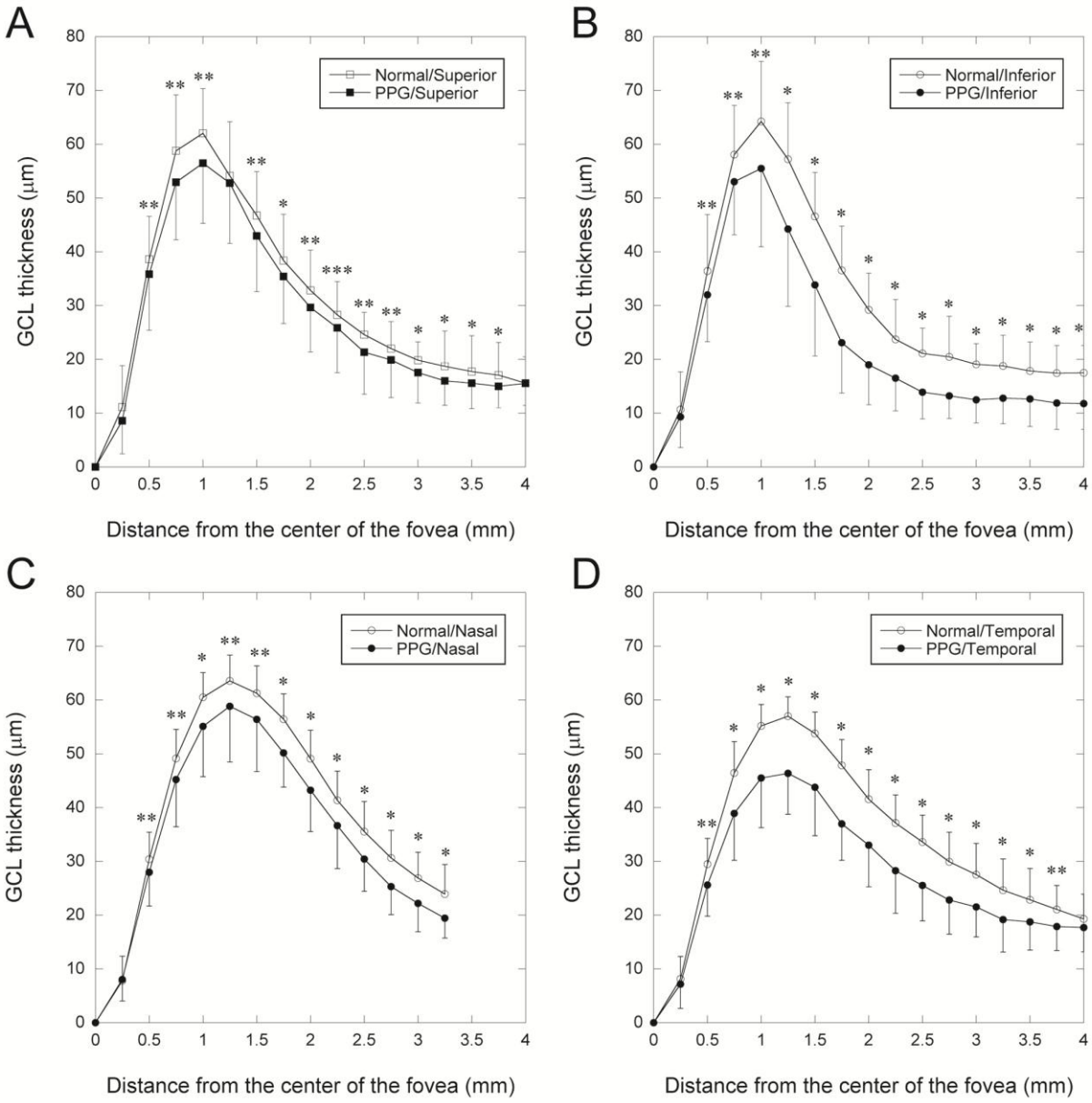
A
Normal/Superior
PPG/Superior
GCL thickness (μm)
Distance from the center of the fovea (mm)
B
Normal/Inferior
PPG/Inferior
GCL thickness (μm)
Distance from the center of the fovea (mm)
C
Normal/Nasal
PPG/Nasal
GCL thickness (μm)
Distance from the center of the fovea (mm)
D
Normal/Temporal
PPG/Temporal
GCL thickness (μm)
Distance from the center of the fovea (mm)

Figure 4

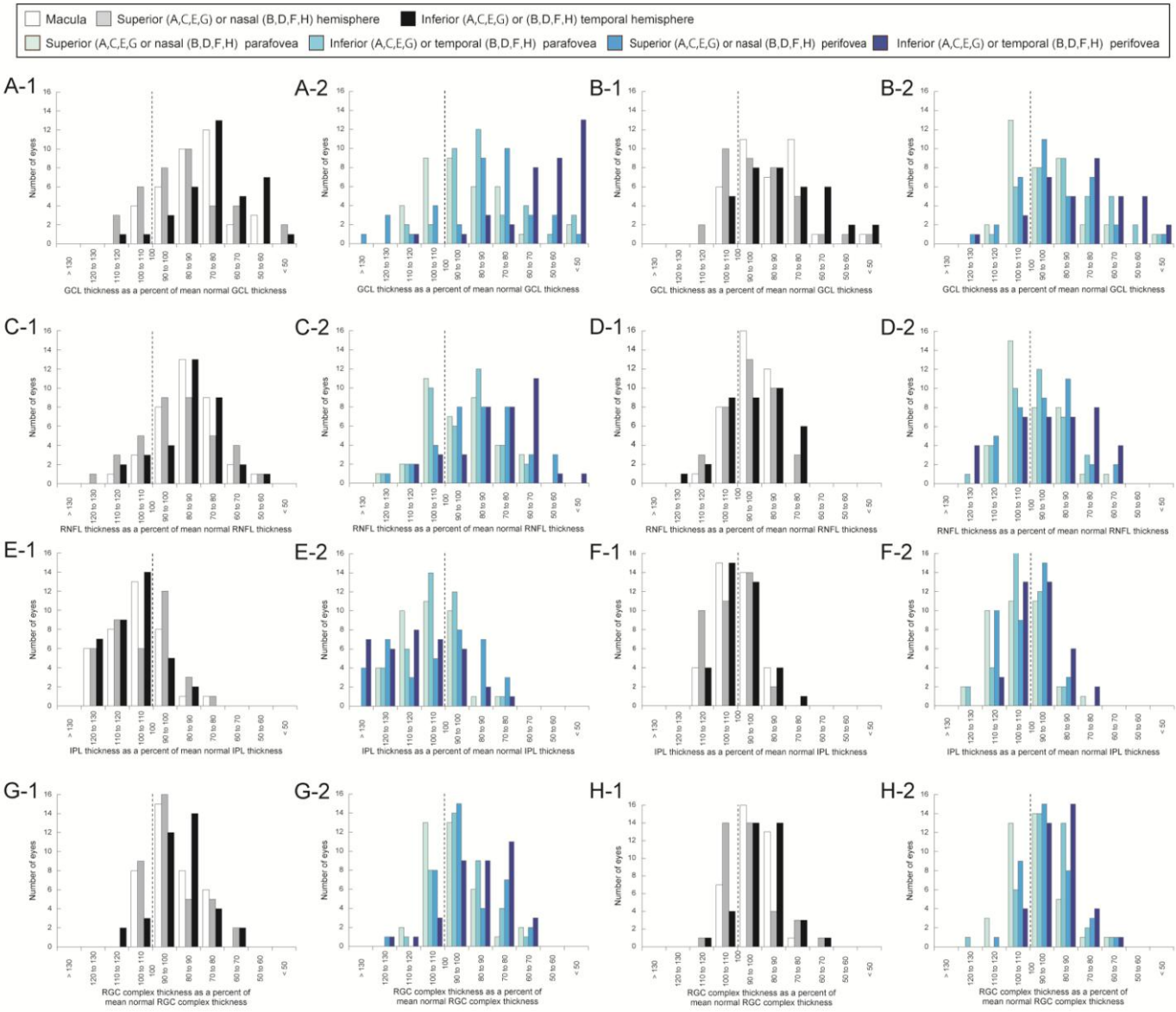
Macula
Superior (A,C,E,G) or nasal (B,D,F,H) hemisphere
Inferior (A,C,E,G) or (B,D,F,H) temporal hemisphere
Superior (A,C,E,G or nasal (B,D,F,H) parafovea
Inferior (A,C,E,G) or temporal (B,D,F,H) parafovea
Superior (A,C,E,G) or nasal (B,D,F,H) perifovea
Inferior (A,C,E,G) or temporal (B,D,F,H) perifovea
A-1
A-2
B-1
B-2
C-1
C-2
D-1
D-2
E-1
E-2
F-1
F-2
G-1
G-2
H-1
H-2
Number of eyes
GCL thickness as a percent of mean normal GCL thickness
RNFL thickness as a percent of mean normal RNFL thickness
IPL thickness as a percent of mean normal IPL thickness
RGC complex thickness as a percent of mean normal RGC complex thickness

Figure 5

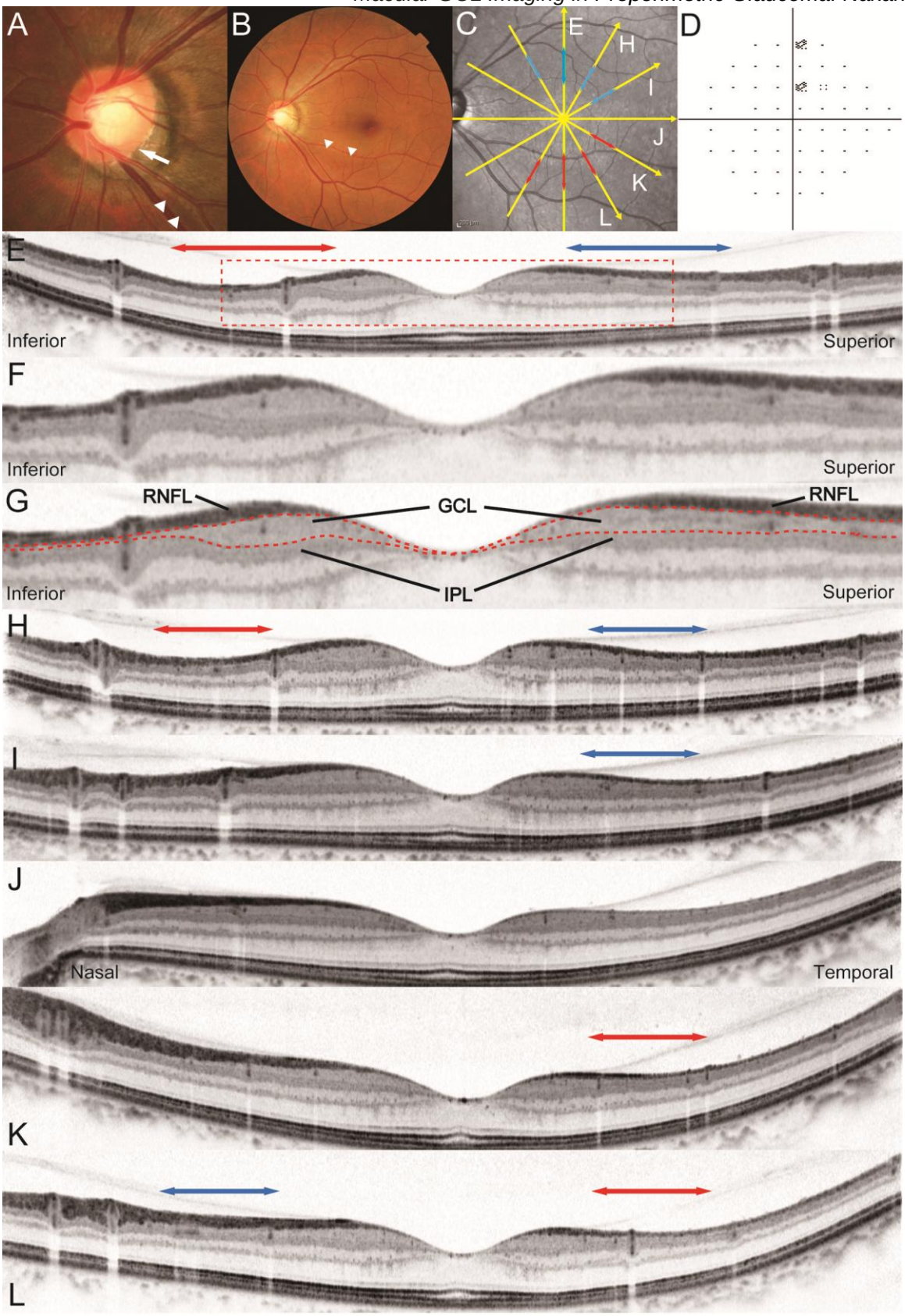
A
B
C
E
H
I
J
K
L
D
E
Inferior
Superior
F
Inferior
Superior
G
RNFL
GCL
RNFL
IPL
Inferior
Superior
H
I
J
Nasal
Temporal
K
L

Figure 6

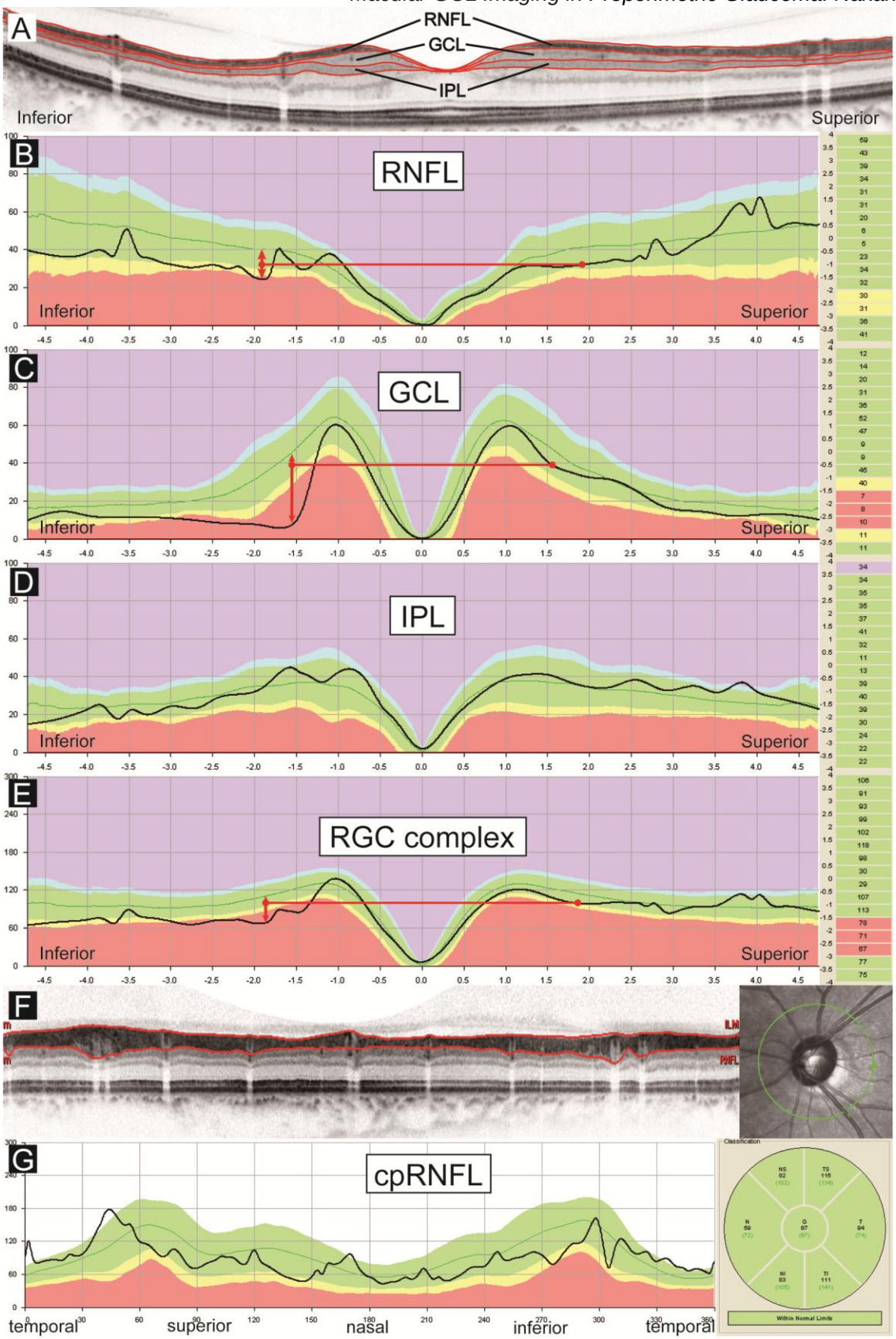
A
RNFL
GCL
IPL
Inferior
Superior
B
RNFL
Inferior
Superior
C
GCL
Inferior
Superior
D
IPL
Inferior
Superior
E
RGC complex
Inferior
Superior
F
G
cpRNFL
temporal
superior
nasal
inferior
temporal

Figure 7

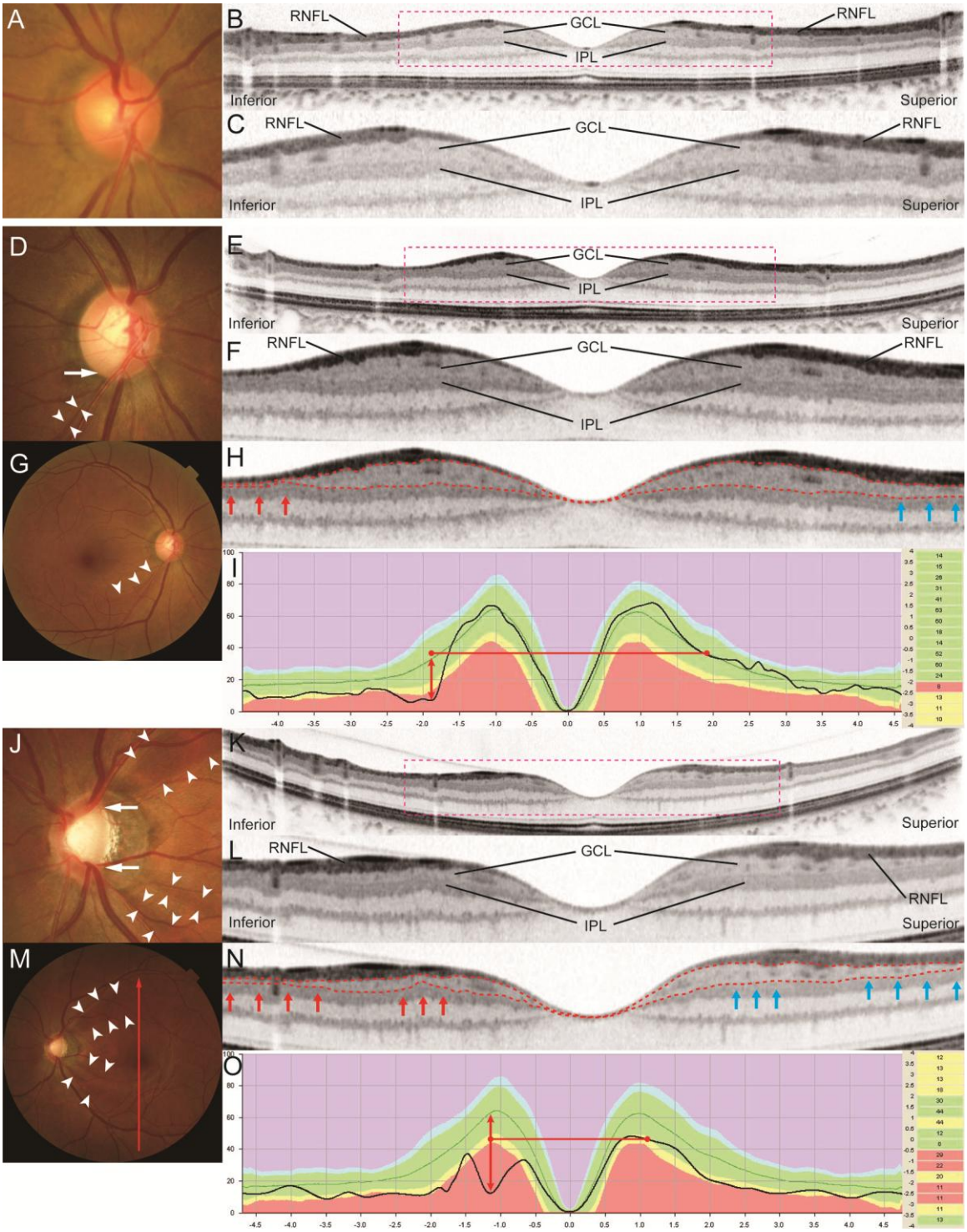
A
B
RNFL
GCL
IPL
RNFL
Inferior
Superior
C
RNFL
GCL
RNFL
IPL
Inferior
Superior
D
E
GCL
IPL
Inferior
Superior
F
RNFL
GCL
RNFL
IPL
G
H
I
J
K
Inferior
Superior
L
RNFL
GCL
RNFL
IPL
Inferior
Superior
M
N
O

Figure 8